Two-proton radioactivity from excited states within the generalized liquid drop model*

Yi Long,[1,2] Yue-Hua Wang,[1,2] Dong Zhan,[1,2] Shuang Li,[1,2] Jun-Gang Deng,[1,2,†] Lin Mu,[1,2,‡] Jun-Hao Cheng,[3,§] and Hong-Fei Zhang[4,¶]

[1]*College of Mathematics and Physics, China Three Gorges University, Yichang 443002, People's Republic of China*
[2]*Center for Astronomy and Space Sciences, China Three Gorges University, Yichang 443002, People's Republic of China*
[3]*Southwestern Institute of Physics, Chengdu, 610003, People's Republic of China*
[4]*School of Physics, Xi'an Jiaotong University, Xi'an 710049, People's Republic of China*

Unlike ground-state two-proton ($2p$) radioactivity, excited-state $2p$ emission is typically characterized by high decay energy and angular momentum, making it an important probe for studying the nuclear structure of extremely proton-rich nuclei. However, describing excited-state $2p$ radioactivity half-lives also poses a challenge to theoretical models. To examine whether the generalized liquid drop model (GLDM) with the improved proximity energy (Prox. 77-Set 13), optimized using ground-state $2p$ radioactivity experimental data, can be extended to describe excited-state $2p$ radioactivity, this work calculates the half-lives for ^{14}O*, ^{17}Ne*, ^{18}Ne*, ^{29}S*, and ^{94}Ag*. The present calculations are compared with experimental data and calculations obtained from the effective liquid drop model (ELDM), the unified fission model (UFM), and the Coulomb and proximity potential model (CPPM). The results calculated by this work are in good agreement with both the experimental data and the results of other theoretical models, validating the applicability of the GLDM with improved proximity energy for describing excited-state $2p$ radioactivity. This work also systematically investigates the dependence of excited-state $2p$ radioactivity half-life on decay energy and angular momentum, which will shed new light on the properties of exotic proton-rich nuclei.

Keywords: $2p$ radioactivity, generalized liquid drop model, half-life, excited-state

I. INTRODUCTION

Two-proton ($2p$) radioactivity is a unique decay mode that plays a crucial role in studying the nuclear structure of extremely proton-rich nuclei near the proton drip line [1–5]. It was first proposed by Goldansky *et al.* [6, 7], who suggested that for the even-Z nuclei near or beyond the proton drip line, one-proton emission is energetically or dynamically forbidden due to the proton pairing effects, leading to the simultaneous emission of two protons instead [6, 7]. The early experiments aimed to investigate $2p$ radioactivity in light nuclei [1]. However, due to the limitations in experimental equipment and detection techniques, no clear evidence of $2p$ radioactivity was obtained [8, 9]. It was not until 2002 that $2p$ radioactivity was first observed in ^{45}Fe at GSI [10] and GANIL [11], providing the first experimental confirmation of this decay mode. Later on, this phenomenon was successively observed in ^{54}Zn [12], ^{48}Ni [13–16], and ^{67}Kr [17]. Overall, these observations not only confirmed the theoretical predictions but also established $2p$ radioactivity as a key probe for studying nuclear structure, including nuclear radius, spin and parity, deformation effect, tensor force effect, and so on [18–22].

The study of excited-state $2p$ radioactivity is a topic of considerable current interest in nuclear physics, which can provide rich nuclear structure information [2, 23–28]. Typically, there are two paths to populate the excited-state of the parent nucleus that can undergo $2p$ radioactivity. One is the β-delayed $2p$ radioactivity proposed by Janecke in 1965 [29], in which a parent nucleus first undergoes β decay to form an intermediate nucleus in an excited-state, which subsequently emits two protons [29]. The other is to populate the excited-state of the parent nucleus through nuclear reactions (such as p-capture, relativistic Coulomb excitation, and fragmentation reactions) including ^{14}O* [30], ^{17}Ne*, ^{18}Ne* [28, 31–34], ^{29}S* [35], and ^{94}Ag* [36].

In contrast to ground-state two-proton ($2p$) radioactivity, excited-state $2p$ emission is typically characterized by high decay energy and angular momentum [2, 23–27]. The high decay energy leads to an extremely short half-life, significantly shorter than that observed for ground-state $2p$ radioactivity [2, 23–27]. This poses significant challenges to the experimental identification of this decay mode and to precise theoretical predictions of the half-life for excited-state $2p$ radioactivity. Moreover, the emitted proton pair may carry away non-zero angular momentum from excited states, offering a unique probe for accessing the single-particle states occupied by the emitted protons [28]. Consequently, the investigation of excited-state $2p$ radioactivity is of considerable interest.

There are three main mechanisms proposed to describe $2p$ radioactivity. (i) Direct $2p$ emission. A strongly correlated proton pair is emitted simultaneously from the parent nucleus [6]. (ii) Sequential emission. The parent nucleus emits a proton, forming an intermediate state, which then emits another proton [37]. (iii) Three-body emission. Two protons are emitted simultaneously from the parent nucleus with a large opening angle [38]. For investigating the characteristics of $2p$ radioactivity, several theoretical mod-

* This work is supported by National Natural Science Foundation of China (Grants No. 12405138, No. 12375137, and No. 12575135), Innovation Program of Southwestern Institute of Physics (Grant No. 202501WDZCQN011), and the Talent Research Startup Fund of the College of Mathematics and Physics, China Three Gorges University (Grant No. 8243322).

† dengjungang@ctgu.edu.cn
‡ mulin@ctgu.edu.cn
§ chengjunhao@swip.ac.cn
¶ zhanghf@xjtu.edu.cn

els are applied within the picture of direct $2p$ emission, such as the density-dependent cluster model (DDCM) [39], the effective liquid drop model (ELDM) [24], the unified fission model (UFM) [25], the generalized liquid drop model (GLDM) [40–42], the Coulomb and proximity potential model (CPPM) [27, 43], the two-potential approach with Skyrme-Hartree-Fock (TPA-SHF) [44], the phenomenological model with a screened electrostatic barrier (SEB) [45], the Gamow-like model (GLM) [46], the Skyrme-Hartree-Fock-Bogoliubov theory (SHFB) [21, 22], and so on [47]. These theoretical models, constructed within the Gamow tunneling picture [48], differ primarily in the construction of the interaction potential between the daughter nucleus and the emitted $2p$ pair. Among these theoretical models, through the introduction of quasi-molecular shape mechanism and proximity energy, the GLDM can continuously describe the shape evolution from the parent nucleus to two separate fragments [49]. The proximity energy is used to describe the interaction in the neck region during the shape evolution and thus plays an essential role in constructing the potential between the daughter nucleus and the emitted $2p$ pair [49]. These features enable the GLDM to be successfully applied to describe various decay processes, including α decay [49–54], fission [55], fusion [56], proton radioactivity [57], and two-proton radioactivity [41]. In our previous work, 15 different versions of the proximity energy were employed within the GLDM to construct the total interaction potential between the daughter nucleus and the emitted $2p$ pair [41]. A systematic study based on the latest experimental ground-state $2p$ radioactivity half-lives was performed to assess the predictive power of these proximity potentials. Among these formalisms, Prox. 77-Set 13 yields the smallest root-mean-square deviation from the experimental data, indicating that this parametrization provides the optimal description of ground-state $2p$ radioactivity half-lives [41].

Excited-state $2p$ radioactivity, which has been observed in nuclei including ^{14}O* [30], ^{17}Ne* [28, 34], ^{18}Ne* [31, 32], ^{29}S* [58], and ^{94}Ag* [36, 59], is typically accompanied by high decay energy and non-zero angular momentum transfer. Consequently, it serves as a probe for studying the dependence of the excited-state $2p$ radioactivity half-life on both angular momentum and decay energy. However, the high angular momentum significantly governs the centrifugal potential, thereby raising the total interaction potential. Meanwhile, the high decay energy may lead to difficulties in determining the classical turning points within the Wentzel-Kramers-Brillouin (WKB) approximation. Therefore, the theoretical description of excited-state $2p$ radioactivity half-lives remains challenging. It is thus of interest to examine whether the GLDM with improved proximity energy Prox. 77-Set 13 parametrization can be extended to effectively describe excited-state $2p$ radioactivity.

In this work, the GLDM with Prox. 77-Set 13 is adopted to study the $2p$ radioactivity half-lives for ^{14}O* [30], ^{17}Ne* [28, 34], ^{18}Ne* [31, 32], ^{29}S* [58], and ^{94}Ag* [36, 59]. The calculations obtained from this work are compared with the experimental data [28, 30–32, 34, 36, 59] and with the results calculated by the ELDM [24], the UFM [25], and the CPPM [27]. The $2p$ radioactivity half-lives calculated by this work are in good agreement with the available experimental data and show satisfactory consistency with calculations taken from three other theoretical models. Furthermore, this work systematically investigates the variation of excited-state $2p$ radioactivity half-lives with decay energy. The dependence of half-life on angular momentum is also examined, with ^{94}Ag* taken as a case.

The organization of this paper is outlined as follows. Section II presents the theoretical framework for the GLDM and $2p$ radioactivity half-life. Section III provides detailed calculations and discussion. The paper concludes with a brief summary in Sec. IV.

II. THEORETICAL FRAMEWORK

A. Generalized liquid drop model

Under the framework of the generalized liquid drop model (GLDM), the total interaction potential includes the following components [49]:

$$E = E_V + E_S + E_C + E_{\rm Prox} + E_l, \tag{1}$$

where E_V, E_S, E_C, $E_{\rm Prox}$, and E_l represent the volume energy, the surface energy, the Coulomb energy, the proximity energy, and the centrifugal potential, respectively.

For one body shapes, E_V, E_S, E_C are calculated by

$$E_V = -15.494(1 - 1.8I^2)A, \tag{2}$$

$$E_S = 17.9439(1 - 2.6I^2)A^{2/3}(S/4\pi R_0^2), \tag{3}$$

$$E_C = 0.6e^2(Z^2/R_0)\times 0.5\int (V(\theta)/V_0)(R(\theta)/R_0)^3 \sin\theta d\theta, \tag{4}$$

here $I = \frac{N-Z}{A}$ represents the relative neutron excess of the parent nucleus. $V(\theta)$ is the electrostatic potential at the surface. R_0 is the radius of the parent nucleus, which can be expressed as follows

$$R_i = 1.28A_i^{1/3} - 0.76 + 0.8A_i^{-1/3}(i = 0, 1, 2). \tag{5}$$

For two body shapes, E_V, E_S, E_C are obtained by

$$E_V = -15.494[(1 - 1.8I_1^2)A_1 + (1 - 1.8I_2^2)A_2], \tag{6}$$

$$E_S = 17.9439[(1 - 2.6I_1^2)A_1^{2/3} + (1 - 2.6I_2^2)A_2^{2/3}], \tag{7}$$

$$E_C = 0.6e^2Z_1^2/R_1 + 0.6e^2Z_2^2/R_2 + e^2Z_1Z_2/r, \tag{8}$$

here A_i, Z_i, R_i, and I_i (i = 1,2) represent the mass numbers, the proton numbers, the radii, and the relative neutron excesses of the emitted $2p$ pair and the daughter nucleus, respectively.

The proximity energy was initially proposed by Blocki to describe the interaction energy in the neck structure after contact in heavy-ion reactions [60]. Subsequently, it was introduced into the GLDM to describe the interaction energy within the neck or gap formed during the separation process between the daughter nucleus and emitted particle in decay processes [49]. In previous work, the capability of the GLDM with 15 different versions of the proximity energy to describe the ground-state $2p$ radioactivity half-lives was examined against the latest experimental data [41]. The calculations with Prox. 77-Set 13 were found to reproduce the experimental half-lives most satisfactorily [41]. The present work examines whether this parametrization can be extended to excited-state $2p$ radioactivity. The Prox. 77-Set 13 [61] is given as follows

$$E_{\rm Prox}(r) = 4\pi\gamma b\bar{R}\phi(\xi), \tag{9}$$

where γ is the surface energy coefficient, defined by

$$\gamma = \gamma_0(1 - K_s A_s^2), \tag{10}$$

here $A_s \equiv \frac{N-Z}{N+Z}$ represents the asymmetry parameter. In this work, $\gamma_0 = 0.911445$ (MeV/fm^2) and $K_s = 2.2938$ [61]. The mean curvature radius $\bar{R}$ can be calculated by

$$\bar{R} = \frac{C_1 C_2}{C_1 + C_2}, \tag{11}$$

here the matter radii C_1 and C_2 for the emitted $2p$ pair and the daughter nucleus are given by

$$C_i = R_i[1 - (\frac{b}{R_i})^2](i = 1, 2). \tag{12}$$

The universal function $\phi(\xi)$ can be expressed as

$$\phi(\xi) = \begin{cases} -\frac{1}{2}(\xi - \xi_0)^2 - 0.0852(\xi - \xi_0)^3, & 0 < \xi \leq 1.2511, \\ -3.347\exp(\frac{-\xi}{0.75}), & \xi \geq 1.2511, \end{cases} \tag{13}$$

here ξ_0 = 2.54 and $\xi = \frac{r - C_1 - C_2}{b}$ serve as the separation distance between the surfaces of the emitted $2p$ pair and the daughter nucleus. The width parameter b is taken as unity.

The centrifugal potential is expressed as

$$E_l(r) = \frac{\hbar^2 l(l+1)}{2\mu r^2}, \tag{14}$$

where l corresponds to the angular momentum taken away by the emitted $2p$ pair.

B. The $2p$ radioactivity half-life

Under the picture of direct diproton emission [6], $2p$ radioactivity is treated as a process in which a strongly correlated proton pair is emitted after tunneling through the Coulomb barrier of the parent nucleus [6]. This tunneling process is governed by the same quantum tunneling mechanism as α decay [62–72], proton radioactivity [57, 73], and cluster radioactivity [74–78].

The $2p$ radioactivity half-life can be calculated with the decay constant λ as

$$T_{1/2} = \frac{\ln 2}{\lambda}. \tag{15}$$

The decay constant λ can be given by

$$\lambda = S_{2p}\nu P, \tag{16}$$

here S_{2p} is the spectroscopic factor for the ^{2}He cluster within the parent nucleus, which is derived from the cluster overlap approximation [42, 79]

$$S_{2p} = G^2[A/(A-2)]^{2n}\chi^2, \tag{17}$$

where $G^2 = (2n)!/[2^{2n}(n!)^2]$ [80], and n corresponds to the average principal proton oscillator quantum number, which can be obtained by $n \approx (3Z)^{1/3} - 1$ [81]. Here, χ^2 is the proton overlap function [42]. In the previous work, the value of χ^2 was determined to be 0.0275 by fitting the experimental data of ground-state $2p$ radioactivity [41].

The assault frequency ν can be obtained by

$$\nu = \frac{1}{2R_0}\sqrt{\frac{2E_{2p}}{M_{2p}}}, \tag{18}$$

where E_{2p} and M_{2p} denote the kinetic energy and the mass of the emitted $2p$ pair, respectively.

Within the WKB approximation, the barrier penetrating probability P is calculated by

$$P = \exp[-\frac{2}{\hbar}\int_{r_{\rm in}}^{r_{\rm out}}\sqrt{2B(r)[E(r) - E_{\rm sphere}]}dr], \tag{19}$$

where r is the distance between the center of mass of the emitted $2p$ pair and the daughter nucleus. The classical turning points ($r_{\rm in}$ and $r_{\rm out}$) can be obtained by solving $E(r_{\rm in}) = E(r_{\rm out}) = Q_{2p}$. $B(r) = \mu$ is defined as the reduced mass between the emitted $2p$ pair and the daughter nucleus.

III. RESULTS AND DISCUSSION

Unlike ground-state $2p$ radioactivity, excited-state $2p$ emission is typically characterized by high decay energy and nonzero angular momentum transfer [2, 23–28]. This poses significant challenges for theoretical models in describing the corresponding half-lives. The present work examines the capability of the GLDM with the improved proximity energy

TABLE 1. Experimental data and calculated $2p$ radioactivity half-lives for ^{14}O*, ^{17}Ne*, ^{18}Ne*, ^{29}S*, and ^{94}Ag*. Theoretical calculations are performed by this work (the GLDM with Prox. 77-Set 13), the ELDM [24], the UFM [25], and the CPPM [27], respectively.

$2p$ radioactivity	$j_i^\pi \to j_f^\pi$	l	Q_{2p} (MeV)	$\log_{10}T_{1/2}$ (s)				
				Expt	This work	ELDM [24]	UFM [25]	CPPM [27]
^{14}O$^* \to ^{12}$C	$2^+ \to 0^+$ [30]	2	1.20 [30]	> -16.12 [30]	-16.07	-15.49	-16.02	-16.65
	$2^+ \to 0^+$ [30]	2	3.15 [30]	–	-18.91	-18.22	-18.87	-19.25
	$4^+ \to 0^+$ [30]	4	3.35 [30]	–	-16.67	-16.25	-15.96	-17.53
^{17}Ne$^* \to ^{15}$O	$3/2^- \to 1/2^-$ [28]	2	0.35 [28, 34]	> -10.59 [28]	-7.36	-6.98	-7.11	-8.11
	$5/2^- \to 1/2^-$ [28]	2	0.82 [28, 34]	–	-12.95	-12.41	-12.73	-13.54
	$1/2^+ \to 1/2^-$ [28]	1	0.97 [28, 34]	–	-14.84	-14.20	-14.69	-15.41
^{18}Ne$^* \to ^{16}$O	$2^+ \to 0^+$ [31]	2	0.59 [31]	–	-11.09	-10.59	-10.91	-11.82
	$1^- \to 0^+$ [31]	1	1.63 [31]	$-16.15^{+0.06}_{-0.06}$ [31, 32]	-17.15	-16.34	-16.79	-17.56
^{29}S$^* \to ^{27}$Si	$- \to 5/2^+$ [82]	0	1.72∼2.52 [58]	–	$-16.53 \sim -14.32$	$-15.50 \sim -13.40$	$-16.40 \sim -14.30$	$-16.85 \sim -14.78$
	$- \to 5/2^+$ [82]	0	4.32∼5.12 [58]	–	$-19.58 \sim -18.96$	$-18.40 \sim -17.80$	$-18.90 \sim -18.50$	$- \sim -19.04$
^{94}Ag$^* \to ^{29}$Rh*	$21^+ \to 11^+$ [36]	6∼10 [36]	1.90 [36]	$1.90^{+0.38}_{-0.20}$ [36]	$8.81 \sim 13.94$	$9.42 \sim 14.63$	$9.38 \sim 15.21$	$6.25 \sim 11.89$
			1.98 [59]	–	$7.96 \sim 13.07$	$8.61 \sim 13.80$	$8.56 \sim 14.37$	$5.45 \sim 11.07$
			2.05 [59]	–	$7.28 \sim 12.37$	$7.95 \sim 13.11$	$7.89 \sim 13.68$	$4.79 \sim 10.39$
			3.45 [59]	–	$-1.77 \sim 2.99$	$-0.80 \sim 4.04$	$-0.92 \sim 4.56$	$-3.28 \sim 1.41$

Note: For ^{14}O*, ^{17}Ne*, and ^{18}Ne*, l are determined by spin-parity conservation. For ^{29}S*, $l = 0$ is assumed due to undetermined parent nucleus spin and parity. For ^{94}Ag*, l is obtained from the Ref. [36].

Prox. 77-Set 13 parametrization to describe excited-state $2p$ radioactivity, and systematically investigates the impact of these features on the half-life of $2p$ radioactivity.

In this work, the GLDM with the improved proximity energy is extended to calculate the $2p$ radioactivity half-lives for ^{14}O* [30], ^{17}Ne* [28, 34], ^{18}Ne* [31, 32], ^{29}S* [58], and ^{94}Ag* [36, 59]. Table 1 presents the calculations obtained from this work together with those taken from the ELDM [24], the UFM [25], and the CPPM [27]. In Table 1, the first column represents the parent nucleus undergoing excited-state $2p$ radioactivity and the corresponding daughter nucleus. The second column lists the spin and parity values for the parent nuclei and the daughter nuclei. Based on spin-parity conservation, the calculated angular momentum taken away by the emitted $2p$ pair is listed in the third column except for ^{29}S* and ^{94}Ag*. For ^{29}S*, due to its undetermined spin and parity [58], the angular momentum taken away by the emitted $2p$ pair is set to $l = 0$ in this work. For ^{94}Ag*, l is taken from the Ref. [36]. The fourth column contains the experimental decay energy of excited-state $2p$ radioactivity. The fifth column shows the logarithmic $2p$ radioactivity half-lives of experimental data. The sixth to ninth columns present the calculated logarithmic half-lives of excited-state $2p$ radioactivity obtained from this work, the ELDM [24], the UFM [25], and the CPPM [27], respectively.

As shown in Table 1, the present calculations exhibit a consistent trend with those obtained from the ELDM [24], the UFM [25], and the CPPM [27], indicating that the GLDM with the Prox. 77-Set 13 parametrization can be extended to calculate excited-state $2p$ radioactivity half-lives. For ^{14}O*, the excited-state at 7.77 MeV, corresponding to a decay energy of $Q_{2p} = 1.20$ MeV, was populated via the ^{13}N + p reaction [30]. Despite the absence of a distinct signature for $2p$ emission, an upper limit on its decay width of $\Gamma < 6$ eV was determined, corresponding to a lower limit on the experimental $2p$ radioactivity half-life of $\log_{10} T_{1/2} > -16.12$ s for ^{14}O* [30]. From Table 1, it can be observed that the calculations of $2p$ radioactivity for ^{14}O* ($Q_{2p} = 1.20$ MeV) given by this work, the ELDM [24], and the UFM [25] are all longer than -16.12 s. Meanwhile, this work also calculates the half-lives for $2p$ emission from its higher excited-state at 9.72 MeV (Q_{2p} = 3.15 MeV) and 9.92 MeV (Q_{2p} = 3.35 MeV). The calculations taken from this work and other three theoretical models agree with each other. Moreover, for ^{14}O*, as the decay energy of $2p$ radioactivity increases from 1.20 to 3.15 MeV while the angular momentum remains fixed at $l = 2$, the $2p$ radioactivity half-lives calculated by the present work and three other theoretical models decrease by approximately three orders of magnitude. This reveals a strong sensitivity of the $2p$ radioactivity half-life to the decay energy. However, a contrasting trend emerges as the decay energy increases from 3.15 MeV ($l = 2$) to 3.45 MeV ($l = 4$), with the half-life increasing by nearly two orders of magnitude. The increase in angular momentum from 2 to 4 enhances the centrifugal barrier, thereby reducing the tunneling probability and resulting in a longer half-life. Conversely, the larger decay energy increases the tunneling probability, which shortens the half-life. This contrasting trend reflects the competition between the effects of decay energy and angular momentum on excited-state $2p$ radioactivity half-lives.

For ^{17}Ne*, following population of the first excited-state $(3/2^-)$ via ^{17}Ne+^{197}Au Coulomb excitation, a lower limit of experimental $2p$ radioactivity half-life $\log_{10} T_{1/2} > -10.59$ s for $2p$ emission was obtained [28]. Notably, Table 1 shows that the logarithmic half-lives for ^{17}Ne$^*(3/2^-)$ calculated by this work and other three theoretical models exceed this limit. Furthermore, for ^{17}Ne*, half-lives for the higher excited-state ($5/2^-$ and $1/2^+$) are calculated, and the present results agree well with calculations from the three other theoretical models. Notably, for ^{17}Ne*, a mere 0.47 MeV increase in Q_{2p} from the first $(3/2^-)$ to the second $(5/2^-)$ excited-state at fixed $l = 2$ leads to an decrease in the four types of calculated $2p$ radioactivity half-lives by nearly five orders of magnitude, demonstrating the high sensitivity of the $2p$ radioactivity half-life to decay energy.

Regarding ^{18}Ne*, combining the measurements from

Gomez del Campo *et al.* [31] and Raciti *et al.* [32], the experimental logarithmic half-life for excited-state $2p$ radioactivity is -16.15 s [31, 32]. As shown in Table 1, the calculated logarithmic $2p$ radioactivity half-life given by the present work for ^{18}Ne* ($Q_{2p} = 1.63$ MeV [31]) agrees well with the results yielded by the three other theoretical models, further confirming the reliability of the GLDM with the Prox. 77-Set 13 parametrization. For ^{29}S* [58], owing to the undetermined spin and parity of the parent nucleus, this work assumes zero angular momentum transfer for the emitted proton pair and calculates the corresponding half-life. The present calculations are in excellent agreement with those obtained from the three other theoretical models.

In 2006, Mukha *et al.* reported evidence for $2p$ radioactivity via simultaneous emission from the 21^+ state of ^{94}Ag*, for which the experimental logarithmic $2p$ radioactivity half-life and decay energy are 1.90 s and 1.90 MeV, respectively [36]. Furthermore, based on the analysis of the daughter nucleus spin and considering the possible angular momentum carried by unassigned γ rays, the angular momentum transfer was conservatively constrained to the range of 6∼10 [36]. Subsequently, Kankainen *et al.* measured the masses of ^{92}Rh and ^{94}Pd, from which the Q_{2p} for the ^{94}Ag high-spin isomer are deduced to be 1.98, 2.05, and 3.45 MeV, respectively [59]. As experimental half-lives for ^{94}Ag* at $Q_{2p} = 1.98$, 2.05, and 3.45 MeV remain undetermined, the measured experimental data of $\log_{10} T_{1/2} = 1.90$ s at $Q_{2p} = 1.90$ MeV is adopted as the reference for comparison with the present calculations and three other theoretical models. As shown in Table 1, the present calculations agree well with those taken from the three other theoretical models. Furthermore, for ^{94}Ag*, the calculations given by this work and the three other models reproduce the experimental data well when Q_{2p} is assumed to be 3.45 MeV and angular momentum is in the range of 6∼10. This suggests that the Q_{2p} for ^{94}Ag* may be 3.45 MeV, with angular momentum in the range of 6∼10.

For a clearer comparison, the experimental data of $2p$ radioactivity half-lives [28, 30–32, 36] and the calculations obtained from this work, the ELDM [24], the UFM [25], and the CPPM [27] are presented in Fig. 1. In this figure, the subfigure (a) represents the comparative analysis of logarithmic half-lives for ^{14}O*, ^{17}Ne*, ^{18}Ne*, and ^{29}S* obtained by this work (red open spheres), the ELDM (magenta solid triangles) [24], the UFM (blue open triangles) [25], the CPPM (orange open stars) [27], and experimental data (black solid spheres) [28, 30–32, 36], respectively. The subfigure (b) is the same as (a), but it depicts the logarithmic half-lives for ^{94}Ag*. The black open squares represent the possible experimental data suggested by this work for ^{94}Ag*. From Fig. 1, it can be seen that the results calculated by this work are nearly coincident with those taken from the three other theoretical models. For ^{14}O* [30], ^{17}Ne* [28, 34], and ^{18}Ne* [31, 32], the calculations yielded by the four theoretical models can well reproduce the experimental data. For ^{94}Ag* [36, 59], the calculations given by the four theoretical models can reproduce the experimental data when Q_{2p} is 3.45 MeV and l is 10. This indicates that the GLDM with the improved proximity energy can be successfully extended to calculate the excited-state $2p$ radioactivity half-lives.

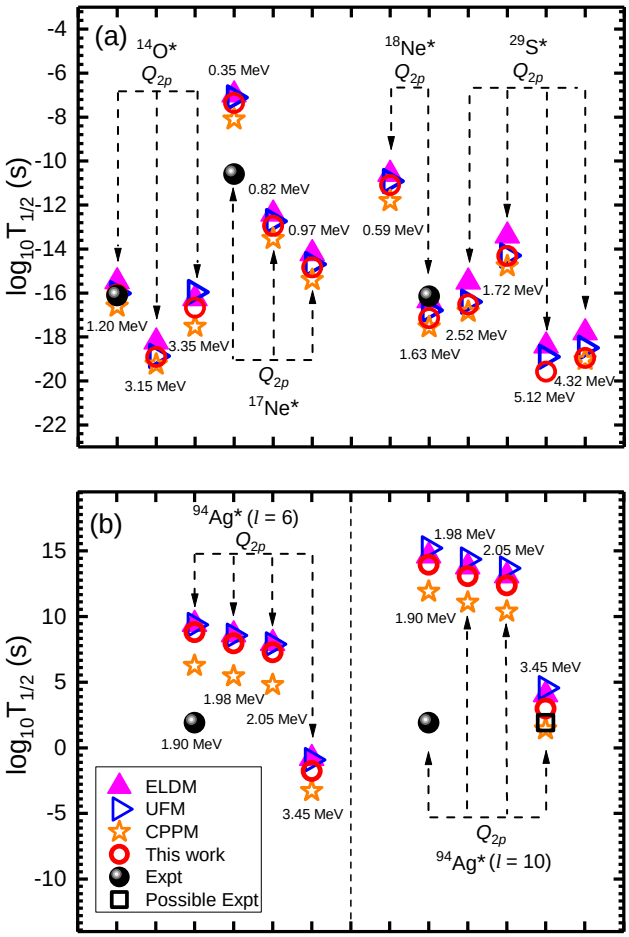

Fig. 1. (Color online) (a) Comparative analysis of logarithmic half-lives for ^{14}O*, ^{17}Ne*, ^{18}Ne*, and ^{29}S* obtained by this work (red open spheres), the ELDM (magenta solid triangles) [24], the UFM (blue open triangles) [25], the CPPM (orange open stars) [27], and experimental data (black solid spheres) [28, 30–32, 36], respectively. (b) Same as (a), but it depicts the logarithmic half-lives for ^{94}Ag*. The black open squares represent the possible experimental data suggested by this work for ^{94}Ag*.

Compared with ground-state $2p$ radioactivity, excited-state $2p$ emission typically exhibits high decay energy [2], rendering the $2p$ radioactivity half-life highly sensitive to variations in Q_{2p}, as shown in Table 1. To further investigate this dependence, the variation of the logarithmic $2p$ radioactivity half-life with decay energy for ^{94}Ag*, calculated by using the GLDM with Prox. 77-Set 13 parametrization, is plotted in Fig. 2. In this figure, the blue stars, the cyan diamonds, the orange pentagons, the magenta squares, and the red circles denote the calculated logarithmic half-lives of ^{94}Ag* as a function of $Q_{2p}^{-1/2}$ for l = 6∼10, respectively. As evident from this figure, the logarithmic half-life for ^{94}Ag* [36, 59] exhibits a linear increase with $Q_{2p}^{-1/2}$. This trend indicates a sharp decrease in the half-life as the decay energy increases.

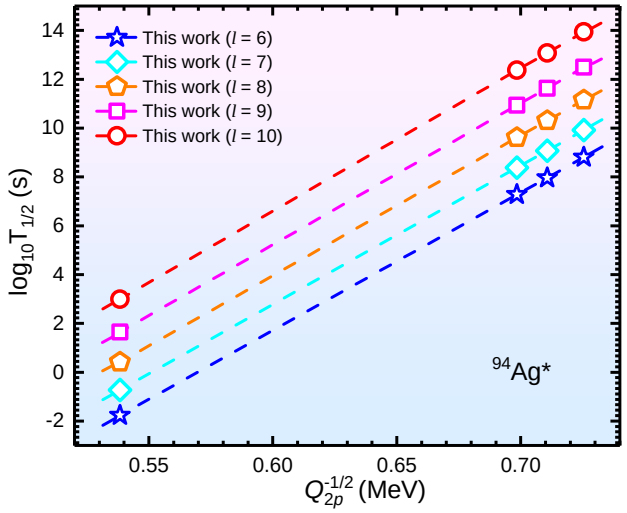

Fig. 2. (Color online) Calculated logarithmic half-lives of ^{94}Ag* as a function of $Q_{2p}^{-1/2}$ for $l = 6$ (blue stars), $l = 7$ (cyan diamonds), $l = 8$ (orange pentagons), $l = 9$ (magenta squares), and $l = 10$ (red circles), respectively. The logarithmic half-lives are calculated using the GLDM with Prox. 77-Set 13 parametrization.

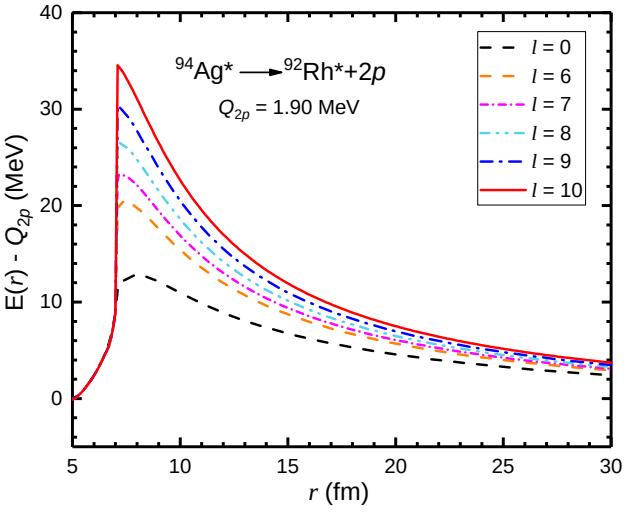

Fig. 3. (Color online) Total interaction potential between the daughter nucleus and the emitted $2p$ pair for ^{94}Ag* ($Q_{2p} = 1.90$ MeV) as a function of radial distance r for various angular momenta, calculated with the GLDM using the Prox. 77-Set 13 parametrization.

Notably, as the decay energy rises from 2.05 to 3.45 MeV, for fixed angular momentum ($l = 6$), the logarithmic half-life calculated in this work decreases from 7.28 to -1.77 s. This can be attributed to the enhanced tunneling probability at higher decay energy, which shortens the half-life. This clearly demonstrates the high sensitivity of excited-state $2p$ radioactivity half-lives to decay energy. Furthermore, a linear relationship is found between the logarithmic half-life and $Q_{2p}^{-1/2}$. This supports the interpretation that $2p$ radioactivity proceeds via quantum tunneling.

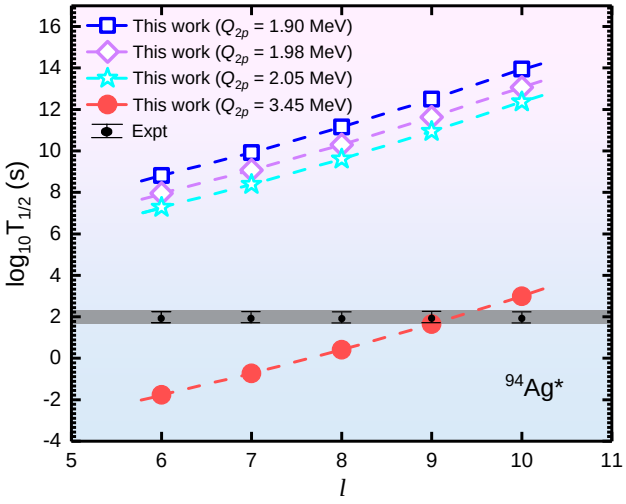

Fig. 4. (Color online) Calculated logarithmic half-lives of ^{94}Ag* as a function of angular momentum for $Q_{2p} = 1.90$ MeV (blue open squares), $Q_{2p} = 1.98$ MeV (purple open diamonds), $Q_{2p} = 2.05$ MeV (cyan open stars), and $Q_{2p} = 3.45$ MeV (red solid circles), respectively. The calculations are obtained by using the GLDM with Prox. 77-Set 13 parametrization. The shaded region represents the experimental half-life.

Excited-state $2p$ emission typically involves non-zero angular momentum transfer [24, 28]. Therefore, investigating excited-state $2p$ radioactivity provides insights into the sensitivity of the half-life to angular momentum [24, 28], and enables the identification of the single-particle states occupied by the emitted protons [28]. For ^{94}Ag* (Q_{2p} = 1.90 MeV) [36], Fig. 3 is plotted to clearly illustrate the influence of angular momentum on the total interaction potential between the daughter nucleus and the emitted $2p$ pair. The figure shows that as the angular momentum increases, the barrier peak of the total interaction potential shifts to the left and the potential curves are significantly raised. This phenomenon indicates that as the angular momentum increases, the centrifugal potential rises significantly, thereby raising the total interaction potential between the daughter nucleus and the emitted $2p$ pair. This suppresses the tunneling probability by increasing the total interaction potential, and ultimately, prolonging the half-life of excited-state $2p$ radioactivity.

To further investigate the relationship between $2p$ radioactivity half-life and angular momentum at fixed decay energy, the logarithmic half-lives for ^{94}Ag*, calculated by using the GLDM with Prox. 77-Set 13 parametrization, are plotted as a function of angular momentum for $Q_{2p} = 1.90$ MeV (blue open squares), $Q_{2p} = 1.98$ MeV (purple open diamonds), $Q_{2p} = 2.05$ MeV (cyan open stars), and $Q_{2p} = 3.45$ MeV (red solid circles) in Fig. 4. This figure shows that for fixed decay energy, the logarithmic half-life increases continuously with angular momentum. For ^{94}Ag* [36], Mukha *et al.* conservatively estimated the angular momentum transfer to be in the range of 6∼10 [36]. Within this range, the GLDM with the Prox. 77-Set 13 parametrization is used to calculate the $2p$ radioactivity half-life of ^{94}Ag*. As shown in Fig. 4, the calcu-

lations reproduce the experimental data for $Q_{2p} = 3.45$ MeV and $l = 8 \sim 10$. Furthermore, based on spin-parity conservation and the tentative assignments of 21^+ for the parent nucleus and 11^+ for the daughter nucleus, the angular momentum transfer is deduced to be $l = 10$. By combining the present calculations with experimental data and spin-parity conservation, this work suggests that the $2p$ emission from ^{94}Ag* carries away angular momentum $l = 10$. Due to these unique decay characteristics, excited-state $2p$ radioactivity serves as an important tool for extracting nuclear structure information [2, 23–27]. Although its relatively short $2p$ radioactivity half-life poses experimental challenges, the study of this decay mode remains essential and valuable.

IV. SUMMARY

In summary, excited-state $2p$ radioactivity is generally characterized by high decay energy and non-zero angular momentum transfer, in contrast to ground-state $2p$ emission, providing an important probe for exploring the nuclear structure of extremely proton-rich nuclei. Nevertheless, the theoretical description of the corresponding $2p$ radioactivity half-lives remains challenging. This work examines whether the generalized liquid drop model with the improved proximity energy Prox. 77-Set 13 parametrization can be extended to excited-state $2p$ radioactivity. Calculations are performed for ^{14}O*, ^{17}Ne*, ^{18}Ne*, ^{29}S*, and ^{94}Ag*, and compared with experimental data and calculations given by the effective liquid drop model, the unified fission model, and the Coulomb and proximity potential model. The present results reproduce the experimental data well and agree with other theoretical results. Taking ^{94}Ag* as an example, this work systematically investigates the sensitivity of $2p$ radioactivity half-lives to variations in $2p$ decay energy and angular momentum. The $2p$ radioactivity half-life is found to be highly sensitive to $2p$ decay energy and exhibits a positive correlation with angular momentum. Furthermore, by comparing with experimental data and incorporating spin-parity conservation, this work suggests that the most probable $2p$ decay energy and angular momentum for ^{94}Ag* are $Q_{2p} = 3.45$ MeV and $l = 10$, respectively. This study provides a reference for future experimental investigations of excited-state $2p$ radioactivity, shedding new light on the properties of exotic proton-rich nuclei.

[1] M. Pfutzner, I. Mukha, S. M. Wang, Two-proton emission and related phenomena. Prog. Part. Nucl. Phys. **132**, 104050 (2023). https://doi.org/10.1016/j.ppnp.2023.104050

[2] L. Zhou, S. M. Wang, D. Q. Fang et al., Recent Progress in Two-Proton Radioactivity. Nucl. Sci. Tech. **33**, 105 (2022). https://doi.org/10.1007/s41365-022-01091-1

[3] Y. G. Ma, Multi-proton emission at the limits of nuclear stability: challenges for extreme open quantum systems. Nucl. Sci. Tech. **36**, 236 (2025). https://doi.org/10.1007/s41365-025-01831-z

[4] B. Blank, M. Ploszajczak, Two-proton radioactivity. Rep. on Prog. Phys. **71**, 046301 (2008). https://doi.org/10.1088/0034-4885/71/4/046301

[5] L. S. Ferreira, M. C. Lopes, E. Maglione, Decays of drip line nuclei. Prog. Part. Nucl. Phys. **59**, 418 (2007). https://doi.org/10.1016/j.ppnp.2007.01.011

[6] V. I. Goldansky, On neutron-deficient isotopes of light nuclei and the phenomena of proton and two-proton radioactivity. Nucl. Phys. **19**, 482 (1960). https://doi.org/10.1016/0029-5582(60)90258-3

[7] V. I. Goldansky, Two-proton radioactivity. Nucl. Phys. **27**, 648 (1961). https://doi.org/10.1016/0029-5582(61)90309-1

[8] W. Whaling, Magnetic Analysis of the $\mathrm{Li}^6(\mathrm{He}^3, t)\mathrm{Be}^6$ Reaction. Phys. Rev. **150**, 836 (1966). https://doi.org/10.1103/PhysRev.150.836

[9] G. J. KeKelis, M. S. Zisman, D. K. Scott et al., Masses of the unbound nuclei ^{16}Ne, ^{15}F, and ^{12}O. Phys. Rev. C **17**, 1929 (1978). https://doi.org/10.1103/PhysRevC.17.1929

[10] M. Pfützner, E. Badura, C. Bingham et al., First evidence for the two-proton decay of ^{45}Fe. Eur. Phys. J. A **14**, 279 (2002). https://doi.org/10.1140/epja/i2002-10033-9

[11] J. Giovinazzo, B. Blank, M. Chartier et al., Two-Proton Radioactivity of ^{45}Fe. Phys. Rev. Lett. **89**, 102501 (2002). https://doi.org/10.1103/PhysRevLett.89.102501

[12] B. Blank, A. Bey, G. Canchel et al., First Observation of ^{54}Zn and its Decay by Two-Proton Emission. Phys. Rev. Lett. **94**, 232501 (2005). https://doi.org/10.1103/PhysRevLett.94.232501

[13] M. Pomorski, M. Pfutzner, W. Dominik et al., Proton spectroscopy of ^{48}Ni,^{46} Fe, and ^{44}Cr. Phys. Rev. C **90**, 014311 (2014). https://doi.org/10.1103/PhysRevC.90.014311

[14] C. Dossat, A. Bey, B. Blank et al., Two-proton radioactivity studies with ^{45}Fe and ^{48}Ni. Phys. Rev. C **72**, 054315 (2005). https://doi.org/10.1103/PhysRevC.72.054315

[15] M. Pomorski, M. Pfutzner, W. Dominik et al., First observation of two-proton radioactivity in ^{48}Ni. Phys. Rev. C **83**, 061303(R) (2011). https://doi.org/10.1103/PhysRevC.83.061303

[16] A. Ortega Moral, S. M. Wang, J. Giovinazzo et al., Two-proton correlations in the decay of ^{48}Ni and ^{45}Fe. Phys. Rev. C **112**, L061302 (2025). https://doi.org/10.1103/kqb5-z2xy

[17] T. Goigoux, P. Ascher, B. Blank et al., Two-Proton Radioactivity of ^{67}Kr. Phys. Rev. Lett. **117**, 162501 (2016). https://doi.org/10.1103/PhysRevLett.117.162501

[18] A. T. Kruppa, W. Nazarewicz, Gamow and R-matrix approach to proton emitting nuclei. Phys. Rev. C **69**, 054311 (2004). https://doi.org/10.1103/PhysRevC.69.054311

[19] S. M. Wang, W. Nazarewicz, Puzzling Two-Proton Decay of ^{67}Kr. Phys. Rev. Lett. **120**, 212502 (2018). https://doi.org/10.1103/PhysRevLett.120.212502

[20] J. D. Jiang, X. Liu, D. M. Zhang et al., A simple model for two-proton radioactivity. Chin. Phys. C **48**, 104108 (2024). https://doi.org/10.1088/1674-1137/ad6417

[21] Y. Z. Wang, F. Z. Xing, J. P. Cui et al., Roles of tensor force and pairing correlation in two-proton radioactivity of halo nuclei. Chin. Phys. C **47**, 084101 (2023). https://doi.org/10.1088/1674-1137/acd680

[22] Y. Z. Wang, F. Z. Xing, W. H. Zhang et al., Tensor force effect on two-proton radioactivity of ^{18}Mg and ^{20}Si. Phys. Rev. C **110**, 064305 (2024). https://doi.org/10.1103/PhysRevC.110.064305

[23] Y. G. Ma, D. Q. Fang, X. Y. Sun et al., Different mechanism of two-proton emission from proton-rich nuclei ^{23}Al and ^{22}Mg. Phys. Lett. B **743**, 306 (2015). https://doi.org/10.1016/j.physletb.2015.02.066

[24] F. Z. Xing, J. P. Cui, Y. Z. Wang et al., Two-proton emission from excited states of proton-rich nuclei. Acta. Phys. Sin. **71**, 062301 (2022). https://doi.org/10.7498/aps.71.20211839

[25] F. Z. Xing, J. P. Cui, Y. Z. Wang et al., Two-proton radioactivity of ground and excited states within a unified fission model. Chin. Phys. C **45**, 124105 (2021). https://doi.org/10.1088/1674-1137/ac2425

[26] D. X. Zhu, Y. Y. Xu, L. J. Chu et al., Two-proton radioactivity from excited states of proton-rich nuclei within Coulomb and Proximity Potential Model. Nucl. Sci. Tech. **34**, 130 (2023). https://doi.org/10.1007/s41365-023-01268-2

[27] D. X. Zhu, Y. Y. Xu, H. M. Liu et al., Two-proton radioactivity of the excited state within the Gamow like and modified Gamow-like models. Nucl. Sci. Tech. **33**, 122 (2022). https://doi.org/10.1007/s41365-022-01116-9

[28] M. J. Chromik, P. G. Thirolf, M. Thoennessen et al., Two-proton spectroscopy of low-lying states in ^{17}Ne. Phys. Rev. C **66**, 024313 (2002). https://doi.org/10.1103/PhysRevC.66.024313

[29] J. Janecke, The emission of protons from light neutron-deficient nuclei. Nucl. Phys. **61**, 326 (1965). https://doi.org/10.1016/0029-5582(65)90907-7

[30] C. Bain, P. Woods, R. Coszach et al., Two proton emission induced via a resonance reaction. Phys. Lett. B **373**, 35 (1996). https://doi.org/10.1016/0370-2693(96)00109-8

[31] J. Gomez del Campo, A. Galindo Uribarri, J. R. Beene et al., Decay of a Resonance in ^{18}Ne by the Simultaneous Emission of Two Protons. Phys. Rev. Lett. **86**, 43 (2001). https://doi.org/10.1103/PhysRevLett.86.43

[32] G. Raciti, G. Cardella, M. De Napoli et al., Experimental Evidence of ^{2}He Decay from ^{18}Ne Excited states. Phys. Rev. Lett. **100**, 192503 (2008). https://doi.org/10.1103/PhysRevLett.100.192503

[33] T. Zerguerras, B. Blank, Y. Blumenfeld et al., Study of light proton-rich nuclei by complete kinematics measurements. Eur. Phys. J. A **20**, 389 (2004). https://doi.org/10.1140/epja/i2003-10176-1

[34] M. J. Chromik, B. A. Brown, M. Fauerbach et al., Excitation and decay of the first excited state of ^{17}Ne. Phys. Rev. C **55**, 1676 (1997). https://doi.org/10.1103/PhysRevC.55.1676

[35] X. X. Xu, C. J. Lin, H. M. Jia et al., Correlations of two protons emitted from excited states of ^{28}S and ^{27}P. Phys. Lett. B **727**, 126 (2013). https://doi.org/10.1016/j.physletb.2013.10.029

[36] I. Mukha, E. Roeckl, L. Batist et al., Proton-proton correlations observed in two-proton radioactivity of ^{94}Ag. Nature **439**, 298 (2006). https://doi.org/10.1038/nature04453

[37] K. Miernik, W. Dominik, Z. Janas et al., Two-Proton Correlations in the Decay of ^{45}Fe. Phys. Rev. Lett. **99**, 192501 (2007). https://doi.org/10.1103/PhysRevLett.99.192501

[38] L. V. Grigorenko, R. C. Johnson, I. G. Mukha et al., Two-proton radioactivity and three-body decay: General problems and theoretical approach. Phys. Rev. C **64**, 054002 (2001). https://doi.org/10.1103/PhysRevC.64.054002

[39] Z. Y. Yuan, D. Bai, Z. Wang et al., Research on two-proton radioactivity in density-dependent cluster model. Sci. Chin. Phys. Mech. Astron. **66**, 222012 (2023). https://doi.org/10.1007/s11433-022-1994-8

[40] G. Royer, Calculation of two-proton radioactivity and application to ^{9}Be, ^{6,7}Li, ^{3,6}He, and ^{2,3}H emissions. Phys. Rev. C **106**, 034605 (2022). https://doi.org/10.1103/PhysRevC.106.034605

[41] Y. Long, S. Li, J. G. Deng et al., Systematic study of two-proton radioactivity half-lives within the generalized liquid drop model with various versions of proximity energies. Phys. Rev. C **112**, 064310 (2025). https://doi.org/10.1103/2dp1-8h6g

[42] J. P. Cui, Y. H. Gao, Y. Z. Wang et al., Two-proton radioactivity within a generalized liquid drop model. Phys. Rev. C **101**, 014301 (2020). https://doi.org/10.1103/PhysRevC.101.014301

[43] K. P. Santhosh, Theoretical studies on two-proton radioactivity. Phys. Rev. C **104**, 064613 (2021). https://doi.org/10.1103/PhysRevC.104.064613

[44] X. Pan, Y. T. Zou, H. M. Liu et al., Systematic study of two-proton radioactivity half-lives using the two-potential and Skyrme-Hartree-Fock approaches. Chin. Phys. C **45**, 124104 (2021). https://doi.org/10.1088/1674-1137/ac2421

[45] Y. T. Zou, X. Pan, X. H. Li et al., Systematic study of two-proton radioactivity with a screened electrostatic barrier. Chin. Phys. C **45**, 104101 (2021). https://doi.org/10.1088/1674-1137/ac1b96

[46] H. M. Liu, X. Pan, Y. T. Zou et al., Systematic study of two-proton radioactivity within a Gamow-like model. Chin. Phys. C **45**, 044110 (2021). https://doi.org/10.1088/1674-1137/abe10f

[47] I. Sreeja, M. Balasubramaniam, An empirical formula for the half-lives of exotic two-proton emission. Eur. Phys. J. A **55**, 33 (2019). https://doi.org/10.1140/epja/i2019-12694-5

[48] Gamow, G. Zur Quantentheorie des Atomkernes. Z. Phys. **51**, 204-212 (1928). https://doi.org/10.1007/BF01343196

[49] G. Royer, Alpha emission and spontaneous fission through quasi-molecular shapes. J. Phys. G: Nucl. Part. Phys. **26**, 1149 (2000). https://doi.org/10.1088/0954-3899/26/8/305

[50] H. F. Zhang and G. Royer, α particle preformation in heavy nuclei and penetration probability. Phys. Rev. C **77**, 054318 (2008). https://doi.org/10.1103/PhysRevC.77.054318

[51] X. J. Bao, H. F. Zhang, H. F. Zhang et al., Systematical calculation of α decay half-lives with a generalized liquid drop model. Nucl. Phys. A **921**, 85 (2014). https://doi.org/10.1016/j.nuclphysa.2013.11.002

[52] H. F. Zhang, G. Royer, Theoretical and experimental α decay half-lives of the heaviest odd-Z elements and general predictions. Phys. Rev. C **76**, 047304 (2007). https://doi.org/10.1103/PhysRevC.76.047304

[53] J. G. Deng, J. X. Li, J. H. Cheng et al., α decay properties of superheavy nuclei based on optimized α decay energies. Chin. Phys. C **49**, 054104 (2025). https://doi.org/10.1088/1674-1137/adb2fa

[54] J. G. Deng, H. F. Zhang, Systematic study of α decay half-lives within the Generalized Liquid Drop Model with various versions of proximity energies. Chin. Phys. C **45**, 024104 (2021). https://doi.org/10.1088/1674-1137/abcc5a

[55] G. Royer, K. Zbiri, Asymmetric fission for ^{70,76}Se and ^{90,94,98}Mo via quasimolecular shapes and related formulas. Nucl. Phys. A **697**, 630 (2002). https://doi.org/10.1016/S0375-9474(01)01265-9

[56] G. Royer, B. Remaud, Static and dynamic fusion barriers in heavy-ion reactions. Nucl. Phys. A **444**, 477 (1985). https://doi.org/10.1016/0375-9474(85)90464-6

[57] J. M. Dong, H. F. Zhang, G. Royer, Proton radioactivity within a generalized liquid drop model. Phys. Rev. C **79**, 054330

(2009). https://doi.org/10.1103/PhysRevC.79.054330
[58] C. J. Lin, X. X. Xu, H. M. Jia et al., Experimental study of two-proton correlated emission from ^{29}S excited states. Phys. Rev. C **80**, 014310 (2009). https://doi.org/10.1103/PhysRevC.80.014310
[59] A. Kankainen, V. V. Elomaa, L. Batist et al., Mass Measurements and Implications for the Energy of the High-Spin Isomer in ^{94}Ag. Phys. Rev. Lett. **101**, 142503 (2008). https://doi.org/10.1103/PhysRevLett.101.142503
[60] J. Blocki, J. Randrup, W. J. Swiatecki et al., Proximity forces. Ann. Phys. **105**, 427 (1977). https://doi.org/10.1016/0003-4916(77)90249-4
[61] K. Pomorski, J. Dudek, Nuclear liquid-drop model and surface-curvature effects. Phys. Rev. C **67**, 044316 (2003). https://doi.org/10.1103/PhysRevC.67.044316
[62] T. Wan, S. L. Tang, Y. B. Qian, α-decay properties of superheavy nuclei with $117 \leq Z \leq 120$ from the systematics of decay chains and isotopic chains. Chin. Phys. C **48**, 034103 (2024). https://doi.org/10.1088/1674-1137/ad1582
[63] A. Cheng, C. Xu, Coupled-channels analysis of α-decay fine structure of superheavy nuclei: Deformed doubly magic shell closures. Phys. Rev. C **110**, 054317 (2024). https://doi.org/10.1103/PhysRevC.110.054317
[64] Y. Wu, R. J. Li, C. Xu, Calibration of the α-decay half-life of ^{146}Sm for the chronology of early solar system. Phys. Lett. B **872**, 140113 (2026). https://doi.org/10.1016/j.physletb.2025.140113
[65] B. S. Cai, C. Qi, C. X. Yuan, High-spin alpha formation beyond ^{208}Pb: Revealing interference phases in quartetting and alpha clustering. Phys. Lett. B **875**, 140358 (2026). https://doi.org/10.1016/j.physletb.2026.140358
[66] B. S. Cai, C. X. Yuan, C. Qi, A universal four-fermion formation framework and odd-even staggering in α decay. Sci. Chin. Phys. Meth. Astron. **69**, 252011 (2026). https://doi.org/10.1007/s11433-025-2911-9
[67] C. Xu, Z. Z. Ren, Favored α-decays of medium mass nuclei in density-dependent cluster model. Nucl. Phys. A **760**, 303 (2005). https://doi.org/10.1016/j.nuclphysa.2005.06.011
[68] D. M. Deng, Z. Z. Ren, N. Wang, Significant improvement of half-life calculation of α decays by considering the nuclear medium effect. Phys. Lett. B **795**, 554 (2019). https://doi.org/10.1016/j.physletb.2019.06.045
[69] B. S. Cai, G. S. Chen, J. Y. Xu et al., α decay half-life estimation and uncertainty analysis. Phys. Rev. C **101**, 054304 (2020). https://doi.org/10.1103/PhysRevC.101.054304
[70] W. M. Seif, G. G. Adamian, N. V. Antonenko et al., Correlations of α-decay properties and isospin-asymmetry. Phys. Rev. C **104**, 014317 (2021). https://doi.org/10.1103/PhysRevC.104.014317
[71] Y. Z. Wang, S. J. Wang, Z. Y. Hou et al., Systematic study of α-decay energies and half-lives of superheavy nuclei. Phys. Rev. C **92**, 064301 (2015). https://doi.org/10.1103/PhysRevC.92.064301
[72] W. H. Zhang, Y. H. Gao, J. P. Cui et al., Roles of spin-orbit interaction and pairing correlation in α decay of ^{210}Po. Phys. Rev. C **112**, 024319 (2025). https://doi.org/10.1103/dw7k-fj9j
[73] H. L. Wang, Z. Wang, D. Bai et al., Effects of nuclear deformation and surface polarization on proton-emission half-lives. Chin. Phys. C **49**, 044111 (2025). https://doi.org/10.1088/1674-1137/ada95e
[74] C. Qi, F. R. Xu, R. J. Liotta et al., Universal Decay Law in Charged-Particle Emission and Exotic Cluster Radioactivity. Phys. Rev. Lett. **103**, 072501 (2009). https://doi.org/10.1103/PhysRevLett.103.072501
[75] M. Balasubramaniam, R. K. Gupta, Heavy-ion emission in spontaneous decays of ^{249,252}Cf nuclei. Phys. Rev. C **60**, 064316 (1999). https://doi.org/10.1103/PhysRevC.60.064316
[76] Z. Wang, Z. Z. Ren, Effects of nuclear surface polarization on exotic cluster radioactivity in trans-lead nuclei. Phys. Rev. C **108**, 024306 (2023). https://doi.org/10.1103/PhysRevC.108.024306
[77] J. G. Deng, J. H. Cheng, X. J. Bao et al., Systematic study of cluster radioactivity within the generalized liquid drop model. Chin. Phys. C **48**, 064101 (2024). https://doi.org/10.1088/1674-1137/ad30ef
[78] Y. Z. Wang, F. Z. Xing, Y. Xiao et al., An improved semi-empirical relationship for cluster radioactivity. Chin. Phys. C **45**, 044111 (2021). https://doi.org/10.1088/1674-1137/abe112
[79] B. A. Brown, Diproton decay of nuclei on the proton drip line. Phys. Rev. C **43**, R1513(R) (1991). https://doi.org/10.1103/PhysRevC.43.R1513
[80] N. Anyas-Weiss, J. Cornell, P. Fisher et al., Nuclear structure of light nuclei using the selectivity of high energy transfer reactions with heavy ions. Phys. Rep. **12**, 201 (1974). https://doi.org/10.1016/0370-1573(74)90045-3
[81] A. Bohr, B. R. Mottelson, Two-proton radioactivity. Nulear Structure (Benjamin, New York, 1969), Vol. 1.
[82] F. G. Kondev, M. Wang, W. J. Huang et al., The NUBASE2020 evaluation of nuclear physics properties. Chin. Phys. C **45**, 030001 (2021). https://doi.org/10.1088/1674-1137/abddae